AMERICAN ACADEMY OF OPHTHALMOLOGY®

Retinomics as a Tool for Glaucoma Prediction

Mayinuer Yusufu, PhD,[1,2,*] *Selena Wei Zhang, MD, PhD,*[3,4,*] *Robert N. Weinreb,*[5] *Chen Zhou, MPH,*[6] *Mengtian Kang, MD, PhD,*[6] *Xianwen Shang, PhD,*[3,4,7] *Mingguang He, MD, PhD,*[3,4,7,8] *Danli Shi, MD, PhD*[3,4,7]

Purpose: To investigate retinomic changes preceding glaucoma onset and explore their predictive value.

Design: A population-based, prospective cohort study.

Participants: A total of 40 949 adults from the UK Biobank, all with eligible color fundus photography (CFP) data and OCT data and without baseline glaucoma, were included in this study.

Methods: We used baseline values of retinomics, a composite set of quantitative retinal imaging biomarkers including 135 retinal vascular measurements extracted with the Retina-based Microvascular Health Assessment System from CFP and 21 OCT-derived retinal layer measurements. After least absolute shrinkage and selection operator feature selection, Cox regression was used to assess associations with incident glaucoma, and a gradient boosting machine model was applied to evaluate predictive performance.

Main Outcome Measures: Glaucoma status.

Results: During a median follow-up of 12.49 years, 653 of 40 949 participants developed glaucoma. After adjusting for age, sex, ethnicity, education, smoking behavior, alcohol consumption, physical activity, hypertension, obesity, glycated hemoglobin, and intraocular pressure, 18 of the 48 least absolute shrinkage and selection operator-identified retinal parameters showed statistically significant associations with incident glaucoma, with each standard deviation change associated with 8.2% to 26.4% increased risk. These findings highlighted novel predictors beyond conventional parameters, including vascular network simplification and inner nuclear layer-related thickening. For a 12.49-year incident glaucoma prediction, simply using age, sex, and retinomic features, we achieved a concordance index of 0.767. After being stratified into 3 risk groups, the highest risk group showed a hazard ratio of 8.72 (95% confidence interval: 6.59–11.54) against the lowest risk group.

Conclusions: Our study revealed retinal vascular and neural alterations associated with increased risk of incident glaucoma. In addition, our study showed that retinomics can serve as an effective biomarker for identifying individuals at high risk of developing glaucoma. The simplicity (age, sex, and basic imaging) of our model along with its satisfactory risk stratification performance for long-term incident glaucoma suggest that it can be used to distinguish those patients who are most suitable for early therapeutic intervention to prevent blindness or severe visual impairment at a population level.

Financial Disclosure(s): Proprietary or commercial disclosure may be found in the Footnotes and Disclosures at the end of this article. *Ophthalmology Science 2026;6:101163*

Supplemental material available at www.ophthalmologyscience.org.

Glaucoma is the leading cause of irreversible blindness, posing a major threat to eye health globally.[1] By 2040, an estimated 112 million people are expected to be affected by glaucoma, placing a substantial economic strain on both individuals and health care systems.[2] Sight loss from glaucoma can often be prevented through early diagnosis and treatment. However, the disease's asymptomatic nature in its early stages often leaves many individuals unaware of its onset, leading to late diagnosis and irreversible damage to the optic nerve.[3,4] In this situation, exploration of novel and robust biomarkers may aid early detection of glaucoma and the prevention of its irreversible late-stage complications.

The application of artificial intelligence for automated segmentation and quantification of color fundus photography (CFP) and OCT has significantly minimized the time and effort required to analyze geometric features in large datasets.[5,6] Previous studies have identified associations between a limited range of retinal vasculature features and glaucoma in CFP-based studies.[7–9] Specifically, reduced retinal vascular caliber and fractal dimension, as well as decreased vascular tortuosity and branching angle, have been linked to glaucomatous status. In parallel, OCT-based investigations have demonstrated corresponding structural alterations, including thinning of the retinal nerve fiber layer (RNFL), ganglion cell-inner plexiform layer (GCIPL), and lamina cribrosa.[10–12]

A recent study has revealed the multidimensional complementary relationship between retinal vascular parameters and neural layer measurements.[13] However, the combined use of retinal vasculature and neural layers for glaucoma risk assessment has yet to be thoroughly explored. Most

http://doi.org/10.1016/j.xops.2026.101163
ISSN 2666-9145/26

previous studies have tended to examine vascular or neural parameters in isolation,[7−12] thereby overlooking potential synergistic effects and complementary information between these 2 domains. Moreover, in clinical practice, the biological relevance of retinal vascular alterations in the pathogenesis of glaucoma has not been fully appreciated. While thinning of the RNFL is routinely monitored,[14] concomitant changes in retinal vasculature are often underemphasized, despite accumulating evidence suggesting that microvascular dysfunction may act as an upstream driver of glaucomatous damage.[15] In addition, many existing studies are limited by relatively small sample sizes, constraining the generalizability of their findings across diverse populations.[16−18] Finally, few investigations have comprehensively integrated multiple retinal parameters to develop long-term, population-based models for glaucoma risk stratification.

Analogous to omics paradigms that capture system-level biological signatures through multidimensional biomarkers, "retinomics" represents an integrative framework for retinal phenotyping. By jointly leveraging multiple retinal imaging modalities and parameters, retinomics enables holistic characterization of retinal structure and microvasculature, encompassing both vascular features (e.g., vessel caliber, tortuosity, and branching architecture) and neural layer attributes (e.g., RNFL and ganglion cell layer thickness) derived from noninvasive imaging.[19] The added value of including vascular metrics in glaucoma assessment is substantial: vascular parameters may serve as early biomarkers of microvascular dysfunction that precedes neural damage, potentially enabling earlier identification of individuals at risk before irreversible optic nerve injury occurs. Furthermore, given the bidirectional complementary relationship between vascular and neural parameters, the integration of vascular and neural information may provide a more comprehensive understanding of glaucoma pathophysiology and enable more precise risk stratification than either modality alone.[13]

Therefore, we hypothesized that a comprehensive retinomics approach incorporating both retinal vascular and neural layer measurements would (1) identify individuals at elevated glaucoma risk more effectively than conventional single-parameter approaches and (2) enable accurate long-term glaucoma risk stratification in a large, diverse population-based cohort. The objective of this study was to investigate the associations between an array of neurovascular retinomics—encompassing large−medium vessels and capillaries identified from CFPs and retinal layers obtained from OCT—and glaucoma, while evaluating their predictive value using data from UK Biobank study.

Methods

Study Population

This study utilized data from the UK Biobank, a large-scale and prospective cohort study that enrolled >500 000 participants aged 40 to 69 years between 2006 and 2010 at baseline.[20] Ocular imaging was introduced at 6 assessment centers in 2009.[21,22] We adhered to the STrengthening the Reporting of OBservational studies in Epidemiology guidelines.[23]

Inclusion and Exclusion Criteria

We excluded participants who withdrew their consent or did not have CFPs or OCT data. Then, images of poor quality were removed: the quality of the CFPs was assessed with Retina-based Microvascular Health Assessment System-fluorescein angiography (FA),[24] and those classified as "Reject" were removed. The quality of OCT data was assessed using the quality control indicators obtained with the Topcon Advanced Boundary Segmentation (TABS) software,[25] and data from low-quality images were removed based on the criteria proposed by Ko et al.[6] Lastly, we excluded those with prevalent glaucoma (Fig 1).

Ethics Approval

The UK Biobank Study received ethical approval from the North West - Haydock Research Ethics Committee (21/NW/0157). This study adhered to the Declaration of Helsinki. All participants provided informed consent at the time of enrollment.

Definition of Neurovascular Retinomics

Retinomics was composed of 135 retinal vascular measurements extracted from CFP and 21 OCT-derived retinal layer measurements. The CFP and OCT images were captured without pupil dilation in a dark room using a 3-dimensional macular volume scan covering a 6 × 6 mm raster pattern, with a scan density of 512 horizontal A-scans per B-scan and 128 B-scans, using Topcon 3D OCT-1000 Mark II system.[21,26] OCT parameters were directly obtained from the UK Biobank, which stated that segmentation was performed using TABS.[25] The TABS algorithm utilizes dual-scale gradient information (combining local Canny edge detection with global axial intensity gradients) and dynamic programming-based shortest path search to automatically identify and segment intraretinal boundaries, demonstrating high accuracy and excellent reproducibility.[27] A total of 52 OCT parameters were initially extracted using TABS, including 8 quality control measures and 44 quantified measurements (available at https://biobank.ndph.ox.ac.uk/showcase/label.cgi?id=100079). To ensure analytical robustness, parameters with >30% missing data were excluded, resulting in 21 OCT-derived metrics for analysis in our study. Retinal vascular parameters were extracted using FA labels trained Retina-based Microvascular Health Assessment System, a deep learning model designed for automatic detection and segmentation of retinal vasculature.[24] The Retina-based Microvascular Health Assessment System-FA model was developed using cross-modality labeling from >90 000 pairs of color fundus and fundus FA images, enabling robust segmentation of retinal vessels at multiple hierarchical levels, achieving high segmentation accuracy (area under curve 0.94−0.97 across multiple external datasets) and demonstrates robust generalizability across different fundus camera models and diseased retinae. The 135 vascular metrics investigated in this study encompassed 2 hierarchical categories stratified based on vessel width quantiles: capillary-level parameters (n = 48) derived from the lower third (lower one-third quantile) of vessel width distribution, representing the finest retinal microvasculature; and large−medium vessel parameters (n = 87) derived from the upper two-thirds (upper two-thirds quantile) of vessel width distribution, representing larger arteriovenous vessels. Both categories covered 5 types of measures including caliber, density, complexity, tortuosity, and branching angles. These 135 and 21 metrics represent a comprehensive, validated panel of retinal features systematically

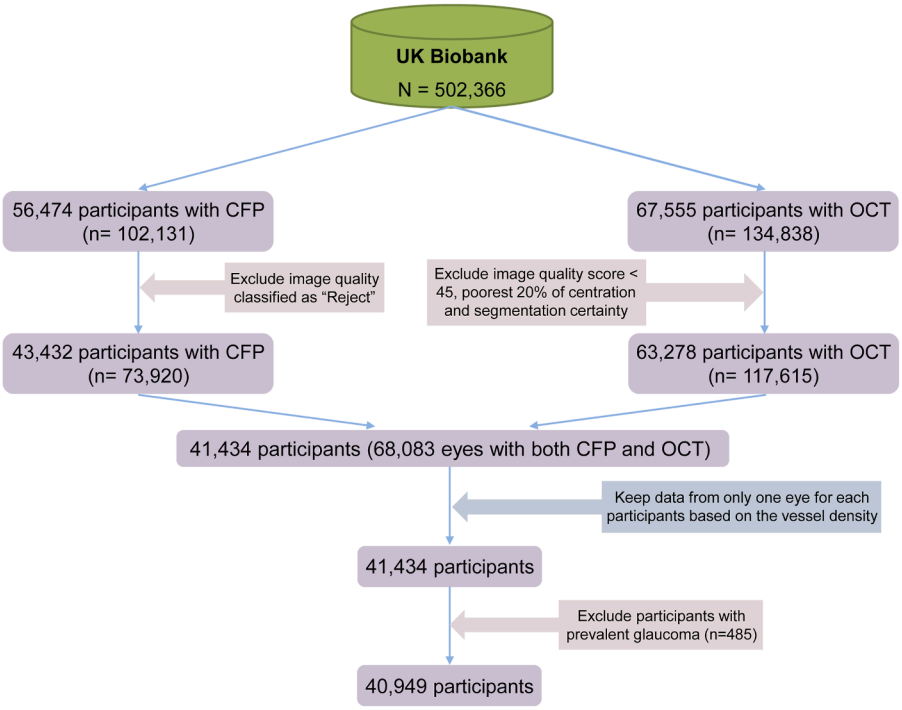

Figure 1. Participants' selection process. CFP = color fundus photography.

developed based on prior research for disease assessment. Detailed definitions and descriptions of these measures have been previously published.[28] The details of retinomic features are shown in Table S1 and Figure S1 (available at www.ophthalmologyscience.org).

Definition of Glaucoma

Glaucoma was defined using the combination of hospital records and self-report. In hospital records, glaucoma was identified through International Classification of Diseases codes: International Classification of Diseases-9 code (365) and International Classification of Diseases-10 code (H40). Self-reported glaucoma was identified using the code 1277 in field 20002. The follow-up period began on the date of image acquisition and ended on the earliest occurrence of death, incident glaucoma events, or October 31, 2022, whichever is the earliest.

Statistical Analysis

Descriptive statistics are reported as mean ± standard deviation for continuous variables and frequencies (percentages) for categorical variables. For numerical variables, *t*-tests were used when the data followed a normal distribution, and Wilcoxon rank-sum tests were applied for nonnormally distributed data. Chi-square (χ^2) tests were used to compare categorical variables.

The handling of retinal parameters involved several steps: parameters with >30% missing values were excluded; outliers were identified and removed using the Robustbase package;[29] missing values were imputed using predictive mean matching in the MICE package; and all parameters were rescaled to standard deviation units to enable comparability across measures and facilitate interpretation of effect sizes.[29]

To reduce the risk of multitesting and overfitting, we performed the least absolute shrinkage and selection operator for feature selection. Selection results can be found in Table S1. The selected variables were then fit into Cox regression to investigate their associations of retinal parameters with incident glaucoma. We tested 4 models: model 1 was the raw model adjusted for false discovery rate; model 2 was adjusted for age, sex, ethnicity, and education; model 3 was adjusted for model 2 plus smoking behavior, alcohol consumption, and physical activity; and model 4 was adjusted for model 3 plus hypertension, obesity, glycated hemoglobin A1c, and intraocular pressure (IOP). The definitions of covariates were presented in Table S2 (available at www.ophthalmologyscience.org). We also explored the correlations between significant arterial and venous parameters identified in model 4 to provide additional insight into their biological interpretations (Table S3 and Fig S2, available at www.ophthalmologyscience.org).

In addition, to develop an integrated predictive model, we employed a gradient boost machine (GBM) model trained on features retained by least absolute shrinkage and selection operator feature selection. This approach can fully leverage the feature selection results and enable the machine learning model to achieve optimal predictive performance. We trained GBM model with Cox construction and 10-fold cross-validation to assess their prediction performance, which is well-suited for handling time-to-event and imbalanced data. The retinomic model used only age and sex with the selected retinomic features. To assess the model's discrimination ability, the concordance index (C-index) was applied, with 95% confidence intervals (CIs) estimated through 1000 bootstrap iterations. Kaplan–Meier survival curves were used to explore survival probabilities, with hazard ratios (HRs) quantifying the relative risk between different groups (low, medium, and high).

Subgroup analyses by age, sex, smoking status, and the presence of obesity were conducted (Tables S4–S7, available at www.ophthalmologyscience.org). To assess the associations of retinomics and incident glaucoma, we divided the retinomic features into quintile and performed Cox regression analyses (Table S8, available at www.ophthalmologyscience.org). Sensitivity analyses on the risk stratification performance of

retinomic model for 10-year risk prediction as well as respective performances of CFP model (age, sex, and selected retinal vasculature measurements) and OCT model (age, sex, and selected retinal nerve layer measurements) were performed (Figs S3 and S4, available at www.ophthalmologyscience.org). All statistical analyses were conducted using R software (version 4.4.1, R Foundation for Statistical Computing).

Results

Characteristics of Participants

Among 502 366 participants, those who withdrew their consent, lacked CFP or OCT data, or had low-quality images were excluded, leaving 41 434 participants. After retaining only the highest quality image for each participant and excluding 485 individuals with prevalent glaucoma, 40 949 participants were included in the final analysis (Fig 1). Among the 40 949 eligible participants at baseline, 653 developed incident glaucoma over a median follow-up of 12.49 years (interquartile range: 12.39−12.64). Table 1 suggests that compared with individuals without glaucoma, those who developed incident glaucoma were significantly older (mean age 60.8 vs. 55.2 years, $P < 0.001$), had more males (49.2% vs. 44.6%, $P = 0.022$) and more smokers (44.8% vs. 43.2%, $P = 0.015$). Additionally, they had lower educational level ($P = 0.002$), higher average systolic blood pressure ($P < 0.001$), and glycated hemoglobin A1c levels ($P < 0.001$).

Association with Prevalent and Incident Glaucoma

Following feature selection using least absolute shrinkage and selection operator, 48 retinal features were incorporated into the regression analysis (25 of 87 large−medium vessel measurements, 13 of 48 capillary measurements, and 10 of 21 neural layer measurements). Detailed results can be found in Table S9 (available at www.ophthalmologyscience.org), while the statistically significant associations in model 4 were visually depicted in Figure 2.

In the raw model, 19 measurements concerning large−medium vessels were significantly linked to incident glaucoma, and 8 measurements showed significance in model 4. Among these parameters in model 4, 1 pertained to caliber measurements, 1 to tortuosity, 3 to complexity, and 3 to density measurements. Specifically, the arc length of nonterminal artery (HR: 1.082, 95% CI: 1.003−1.167) and vein (HR: 1.136, 95% CI: 1.055−1.224), along with the width of the terminal vein (HR: 1.111, 95% CI: 1.028−1.201), exhibited positive associations with the risk of incident glaucoma. Conversely, the remaining measurements demonstrated negative associations, with HRs ranging from 0.869 to 0.917. Tortuosity and complexity measurements were both negatively associated with the risk of incident glaucoma. In contrast, caliber showed a positive association with the risk of incident glaucoma. In terms of density measurements, 2 displayed positive associations, while 1 showed negative associations.

In the raw model and multivariate models, 4 capillary measurements were found to be correlated with incident glaucoma. Among the tortuosity parameters in model 4, which included fractal tortuosity (artery), turning angles (artery), and angle-based tortuosity (vein), there were negative associations with the risk of incident glaucoma. The HRs for these parameters were 0.909 (95% CI: 0.841−0.982), 0.899 (95% CI: 0.834−0.970), and 0.918 (95% CI: 0.847−0.994), respectively. By contrast, the branching angle parameter, specifically junctional exponent deviation (artery), exhibited a positive association with an HR of 1.099 (95% CI: 1.014−1.190).

Following false discovery rate adjustment, 8 of 10 neural layers exhibited significant associations in the raw Cox regression model; however, only 6 showed significance in the fully adjusted model. Specifically, the overall macular thickness, RNFL, and GCIPL demonstrated negative associations with HRs ranging from 0.736 to 0.836. On the other hand, the outer subfields extending from the inner nuclear layer (INL) to the external limiting membrane (ELM) and from the INL to the retinal pigment epithelium, along with the average thickness between the INL and the ELM, displayed positive associations with HRs ranging from 1.103 to 1.124.

Predictive Value of Retinal Biomarkers

The risk stratification capacity of the retinomic model is shown in Figure 3. For the entire follow-up period, the retinomic model exhibited a C-index of 0.767 (95% CI: 0.749−0.785). The Kaplan−Meier survival curves of the retinomic model for the 12.49-year follow-up period were constructed to illustrate survival probabilities over time, along with the HRs used to quantify the relative risk between groups (Fig 3). For the entire follow-up duration, the risk was divided into 3 groups (low, medium, and high). Individuals classified as high risk had an HR of 8.72 (95% CI: 6.59−11.54), while those in the medium-risk group had an HR of 2.7 (95% CI: 1.98−3.68) for incident glaucoma in comparison to individuals in the low-risk group.

Discussion

This study demonstrates that retinomics—comprising 135 retinal vascular geometry and 21 neural layer measurements—can potentially be a powerful tool for the prediction and risk stratification of incident glaucoma. Leveraging data from the 40 949 participants in the UK Biobank, our findings revealed that retinal vascular tortuosity and complexity parameters had negative associations with the incident glaucoma. Additionally, the thinning of macular, RNFL, and GCIPL, and the thickening of outer subfields of INL-ELM, outer subfields of INL-retinal pigment epithelium, and whole INL-ELM, were correlated with an increased risk of incident glaucoma. Furthermore, the retinomic model showed robust risk stratification for early intervention, as evidenced by the performance of GBM model.

Table 1. Baseline Characteristics of Participants

Variables	All (N = 40 949)	Glaucoma-Free (N = 40 296)	Incident Glaucoma (N = 653)	*P* Value
Age (yrs)				
Mean ± SD	55.2 ± 8.19	55.2 ± 8.18	60.8 ± 6.38	**<0.001**
Sex				
Female, n (%)	22 662 (55.3%)	22 330 (55.4%)	332 (50.8%)	**0.022**
Male, n (%)	18 287 (44.7%)	17 966 (44.6%)	321 (49.2%)	
Education				
High, n (%)	14 938 (36.5%)	14 718 (36.5%)	220 (33.7%)	**0.002**
Intermediate, n (%)	20 427 (49.9%)	20 112 (49.9%)	315 (48.2%)	
Low, n (%)	5070 (12.4%)	4960 (12.3%)	110 (16.8%)	
Missing, n (%)	514 (1.3%)	506 (1.3%)	8 (1.2%)	
Smoking behavior				
Never, n (%)	23 258 (56.8%)	22 897 (56.8%)	361 (55.3%)	**0.015**
Previous, n (%)	13 665 (33.4%)	13 421 (33.3%)	244 (37.4%)	
Current, n (%)	4026 (9.8%)	3978 (9.9%)	48 (7.4%)	
Missing, n (%)	232 (0.6%)	228 (0.6%)	4 (0.6%)	
Alcohol consumption				
Never, n (%)	1957 (4.8%)	1914 (4.7%)	43 (6.6%)	0.06
Previous, n (%)	1412 (3.4%)	1386 (3.4%)	26 (4.0%)	
Current, n (%)	37 580 (91.8%)	36 996 (91.8%)	584 (89.4%)	
Missing, n (%)	154 (0.4%)	152 (0.4%)	2 (0.3%)	
BMI (kg/m2)				
Mean ± SD	27.2 ± 4.74	27.2 ± 4.74	27.3 ± 4.37	0.498
Missing, n (%)	211 (0.5%)	209 (0.5%)	2 (0.3%)	
Physical activity				
Low, n (%)	7257 (17.7%)	7148 (17.7%)	109 (16.7%)	0.582
Moderate, n (%)	16 776 (41.0%)	16 508 (41.0%)	268 (41.0%)	
High, n (%)	16 916 (41.3%)	16 640 (41.3%)	276 (42.3%)	
Missing, n (%)	8266 (20.2%)	8125 (20.2%)	141 (21.6%)	
Overall health				
Good/Excellent, n (%)	30 332 (74.1%)	29 868 (74.1%)	464 (71.1%)	0.094
Fair, n (%)	8862 (21.6%)	8699 (21.6%)	163 (25.0%)	
Poor, n (%)	1755 (4.3%)	1729 (4.3%)	26 (4.0%)	
Missing, n (%)	261 (0.6%)	258 (0.6%)	3 (0.5%)	
SBP (mmHg)				
Mean ± SD	136 ± 18.1	136 ± 18.1	140 ± 18.0	**<0.001**
Missing, n (%)	142 (0.3%)	141 (0.4%)	1 (0.2%)	
DBP (mmHg)				
Mean ± SD	81.6 ± 10.0	81.6 ± 10.0	81.9 ± 9.86	0.402
Missing, n (%)	142 (0.3%)	141 (0.4%)	1 (0.2%)	
HbA1c (mmol/mol)				
Mean ± SD	35.7 ± 6.34	35.7 ± 6.30	37.6 ± 8.07	**<0.001**
Missing, n (%)	4011 (9.8%)	3939 (9.8%)	72 (11.0%)	
HDL (mmol/L)				
Mean ± SD	1.48 ± 0.387	1.48 ± 0.388	1.48 ± 0.361	0.948
Missing, n (%)	5023 (12.3%)	4936 (12.2%)	87 (13.3%)	
LDL (mmol/L)				
Mean ± SD	3.54 ± 0.850	3.54 ± 0.850	3.48 ± 0.847	0.066
Missing, n (%)	3337 (8.1%)	3281 (8.1%)	56 (8.6%)	

Data are presented as mean ± SD or N (%). *T*-tests were performed for numerical data with normal distributions and Wilcoxon rank-sum tests for numerical data with nonnormal distributions. The $\chi 2$ test was used for categorical variables. Bold *P* values indicate statistical significance ($P < 0.05$). BMI = body mass index; DBP = diastolic blood pressure; HbA1c = glycated hemoglobin A1c; HDL = high-density lipoprotein; LDL = low-density lipoprotein; SBP = systolic blood pressure; SD = standard deviation.

Negative associations were observed between retinal vascular parameters—such as tortuosity and complexity measurements—and the risk of glaucoma. Previous studies have similarly reported decreased tortuosity and reduced fractal dimension (a measure of complexity) in patients with glaucoma.[8,30,31] Additionally, we noticed that decreased arterial vessel skeleton density was associated with increased risk of incident glaucoma. This finding was also in line with prior OCT angiography and CFP studies, which documented reductions in vessel skeleton density in glaucoma patients.[31,32] A substantial body of evidence has underscored hemodynamic impairments in the optic nerve head, retina, choroid, and retrobulbar circulation in eyes affected by glaucoma.[33] Moreover, vascular and perfusion deficits are associated with glaucoma and glaucoma progression.[34] Such impairments

Category	Retinal features	HR (95% CI)	P-value
Capillary	Junctional exponent deviation (artery)	1.099 (1.014, 1.190)	0.022
Capillary	Fractal tortuosity (artery)	0.909 (0.841, 0.982)	0.016
Capillary	Turning angles (artery)	0.899 (0.834, 0.970)	0.006
Capillary	Angle-based tortuosity (vein)	0.918 (0.847, 0.994)	0.035
Large-medium vessel	Level (artery)	0.917 (0.846, 0.994)	0.035
Large-medium vessel	Turning angles (artery)	0.912 (0.844, 0.986)	0.020
Large-medium vessel	Number of nonterminal points (artery)	0.888 (0.812, 0.971)	0.009
Large-medium vessel	Arc length of nonterminal artery (artery)	1.082 (1.003, 1.167)	0.041
Large-medium vessel	Arc length of nonterminal vein (vein)	1.136 (1.055, 1.224)	0.001
Large-medium vessel	Number of terminal points (vein)	0.869 (0.799, 0.945)	0.001
Large-medium vessel	Width of terminal vein (vein)	1.111 (1.028, 1.201)	0.008
Large-medium vessel	Vessel skeleton density-other (artery)	0.871 (0.799, 0.950)	0.002
Neural layer	Overall macular thickness	0.836 (0.771, 0.907)	0.000
Neural layer	Average RNFL thickness	0.830 (0.763, 0.901)	0.000
Neural layer	Average GCIPL thickness	0.736 (0.680, 0.798)	0.000
Neural layer	INL-ELM thickness of the outer subfield	1.124 (1.039, 1.216)	0.003
Neural layer	Average INL-ELM thickness	1.103 (1.019, 1.193)	0.015
Neural layer	INL-RPE thickness of outer subfield	1.115 (1.028, 1.208)	0.009

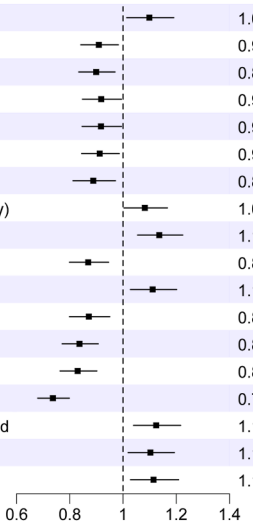

Figure 2. Associations between retinomic features and incident glaucoma in the multivariate model. Model 4 was adjusted for age, sex, ethnicity, education, smoking behavior, alcohol consumption, physical activity, hypertension, obesity, glycated hemoglobin A1c, and intraocular pressure. CI = confidence interval; ELM = external limiting membrane; GCIPL = ganglion cell-inner plexiform layer; HR = hazard ratio; INL = inner nuclear layer; RNFL = retinal nerve fibre layer; RPE = retinal pigment epithelium.

can lead to reductions in vessel skeleton density and complexity. Tortuosity may reflect the optimality state of the microcirculation and the level of ocular perfusion,[30] which are closely tied to the hypoperfusion observed in glaucoma. However, positive associations were also observed in our study. Specifically, the increased arc length of nonterminal artery and vein, along with increased width of terminal vein, might be explained by the compensatory adaptations to high IOP and blood pressure.[35]

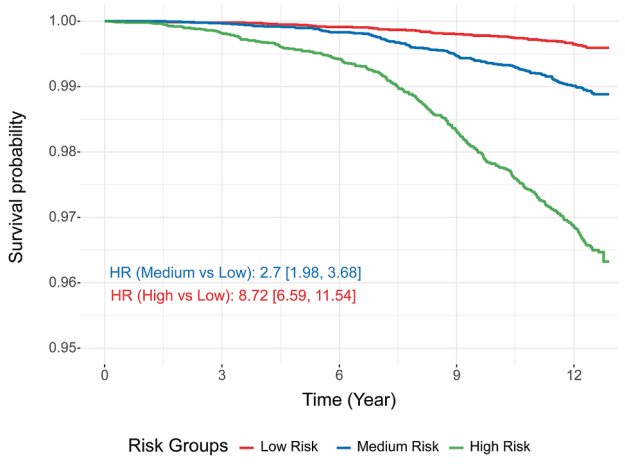

Figure 3. Risk stratification performance of the retinomic model. The 3 Kaplan–Meier survival curves show survival probabilities over time, with HRs to quantify the relative risk between groups. Neurovascular retinal biomarkers predicted 12.5-year incident glaucoma in a population-based cohort. A model using only age, sex, and retinal imaging features showed strong discrimination, supporting retinomics as a tool for early glaucoma risk stratification. HR = hazard ratio.

To gain mechanistic insights into the identified vascular parameters, we examined correlations between significant arterial and venous features identified in model 4 (Table S3). Overall, correlations ranged from modest to moderate. Most capillary-level arterial parameters showed weak correlations with capillary venous features (e.g., turning angles vs. angle-based tortuosity, $r = -0.015$) and minimal associations with large–medium venous parameters, reflecting largely independent microvascular remodeling between arterial and venous capillary beds.[36] In contrast, several large–medium arterial parameters exhibited strong correlations with their venous counterparts, including the number of nonterminal points (artery) versus the number of terminal points (vein) ($r = 0.780$) and vessel skeleton density–other (artery) versus the number of terminal points (vein) ($r = 0.732$), indicating a partially coupled remodeling pattern at the level of larger vessels that may reflect shared hemodynamic regulation and structural adaptation.[36] Taken together, the coexistence of scale-dependent coupling at the large–medium vessel level and relative independence at the capillary level provides a biological rationale for integrating arterial and venous biomarkers across multiple vessel scales. This integration of complementary multiscale vascular information captures complementary aspects of retinal vascular health that would not be fully represented by either vascular compartment alone.

Regarding neural layers, our study identified negative associations between the thickness of inner retinal layers, including the RNFL and GCIPL, and the risk of glaucoma. These findings align with previous research demonstrating that thinning of the RNFL and GCIPL, often resulting from elevated IOP and reduced blood flow, serves as an indicator of structural progression in glaucoma.[30,37–39] In contrast, positive associations with glaucoma were observed in the

outer subfields of the INL-ELM and INL-retinal pigment epithelium, as well as the average thickness of the INL-ELM. Because outer retinal layers, such as the outer plexiform layer and outer nuclear layer, typically remain unchanged in glaucomatous eyes,[40] these findings might be attributed to the thickening of INL.[41] This thickening could result from reactive responses of neuronal or glial cells within the outer retinal layers during glaucoma progression,[41–43] or from microcystic/cystic changes in the INL.[44,45]

The integration of retinomics for early glaucoma risk stratification further highlighted its enhanced predictive value, especially in forecasting long-term incident events. Our retinomic model achieved a C-index of 0.767 (95% CI: 0.749–0.785) over a 12.49-year period. Although established glaucoma prediction models exist, they require multiple routine clinical measurements, including IOP, central corneal thickness, cup/disk ratio, visual field indices, and achieve a C-index of 0.74 over relatively shorter follow-up (5 years).[46] In contrast, our model requires only age, sex, and basic retinal imaging—standard components of glaucoma screening—yet achieves superior long-term predictive performance. Furthermore, the substantial HRs observed in high-risk groups (HR: 8.72) emphasized the clinical applicability of these models in identifying individuals at increased risk for glaucoma. The substantial HR in our high-risk group (HR: 8.72, 95% CI 6.59–11.54 vs. low-risk group) demonstrates strong risk stratification capability for identifying individuals at substantially increased risk for incident glaucoma. Prior studies examining single-layer GCIPL thinning rates in glaucoma suspects showed associations such as HR 2.4 per 1 μm/y faster thinning rate (mean 3.1-year follow-up) or HR 7.13 for progressive GCIPL thinning (mean 5.7-year follow-up).[47,48] While these metrics measure different aspects (continuous thinning rate vs. risk group stratification), our integrated multimodal approach achieves comparable or superior risk discrimination over substantially longer follow-up (12.49 years), highlighting its value for long-term population-level risk stratification. These findings suggested that the integration of dual-modality devices could improve risk stratification accuracy, while maintaining a relatively simple imaging procedure, underscoring their potential as composite biomarkers.

This study underscores the transformative potential of retinomics in advancing early detection, risk stratification, and management of glaucoma. By leveraging comprehensive retinal vascular geometry and neural layer measurements, this large-scale, population-based investigation provides unprecedented insights into the structural and hemodynamic changes associated with glaucoma progression. The integration of CFP and OCT enhances predictive accuracy, as evidenced by the high C-index achieved in the GBM model, emphasizing the clinical utility of combining multimodal imaging for precise risk assessment. These findings show the potential of retinomics-based biomarkers as noninvasive, scalable tools for personalized glaucoma management, aligning with the growing need for early intervention in at-risk populations.

Despite its strengths, this study is not without limitations. First, the cross-sectional design of retinal measurements limits the ability to establish causal relationships between retinal parameters and glaucoma progression. Second, although the UK Biobank cohort provides extensive data, its predominantly European ancestry may limit the generalizability of findings to more diverse populations. Finally, while the GBM model demonstrates robust predictive capabilities, incorporating additional systemic or genetic risk factors may further enhance its precision and applicability.

In conclusion, this study establishes retinomics as a promising framework for early glaucoma risk stratification, integrating vascular geometry and neural layer metrics to capture key structural and hemodynamic changes. Future research should focus on longitudinal validation in diverse populations, exploring causal pathways, and incorporating additional systemic and genetic biomarkers to refine risk prediction.

Acknowledgments

The authors thank the InnoHK HKSAR Government for providing valuable supports. The research work described in this paper was conducted in the JC STEM Lab of Innovative Light Therapy for Eye Diseases funded by The Hong Kong Jockey Club Charities Trust. The Centre for Eye Research Australia receives Operational Infrastructure Support from the Victorian State Government.

Footnotes and Disclosures

Originally received: August 9, 2025.
Final revision: March 7, 2026.
Accepted: March 10, 2026.
Available online: March 19, 2026. Manuscript no. XOPS-D-25-00636.

[1] Centre for Eye Research Australia, Royal Victorian Eye and Ear Hospital, East Melbourne, Australia.

[2] Department of Surgery (Ophthalmology), The University of Melbourne, Melbourne, Australia.

[3] School of Optometry, The Hong Kong Polytechnic University, Kowloon, Hong Kong.

[4] Research Centre for SHARP Vision, The Hong Kong Polytechnic University, Kowloon, Hong Kong.

[5] Hamilton Glaucoma Center, Viterbi Family Department of Ophthalmology and the Shiley Eye Institute, University of California San Diego, La Jolla, California.

[6] Beijing Tongren Eye Center, Beijing Tongren Hospital, Capital Medical University, Beijing, China.

[7] InnoHK, Centre for Eye and Vision Research, 17W Hong Kong Science Park, Hong Kong.

[8] PolyU-Stanford Joint Research Centre for Longitudinal Deep Omics, The Hong Kong Polytechnic University, Kowloon, Hong Kong.

*M.Y. and S.W.Z. contributed equally to this work.

Disclosure(s):

All authors have completed and submitted the ICMJE disclosures form.

The Article Publishing Charge (APC) for this article was paid by The Hong Kong Polytechnic University.

The authors made the following disclosures:

D.S.: Patents — A method for automatically labeling retinal arteries, veins and capillaries in fundus color photos (CN114782338B).

R.N.W.: Grants — Research to Prevent Blindness (New York, NY); Consultant — Retispec, Topcon; Other financial interest — Topcon.

This work was supported by the Start-up Fund for RAPs under the Strategic Hiring Scheme (P0048623) from HKSAR and PolyU-Stanford Joint Research Centre for Longitudinal Deep Omics (LDO) (P0056331). M.Y. is supported by the Melbourne Research Scholarship and Riady Scholarship established by the University of Melbourne. The funding source had no role in the design and conduct of the study; collection, management, analysis, and interpretation of the data; preparation, review, or approval of the manuscript; and decision to submit the manuscript for publication.

HUMAN SUBJECTS: Human subjects were included in this study. The UK Biobank Study received ethical approval from the North West - Haydock Research Ethics Committee (21/NW/0157). This study adhered to the Declaration of Helsinki. All participants provided informed consent at the time of enrollment.

No animal subjects were included in this study.

Author Contributions:

Conception and design: Yusufu, Shang, He, Shi

Data collection: Yusufu, Zhang, He, Shi

Analysis and interpretation: Weinreb, Zhou, Kang, Shang, Shi

Obtained funding: He, Shi

Overall responsibility: Yusufu, Zhang

Abbreviations and Acronyms:
CFP = color fundus photography; **CI** = confidence interval; **ELM** = external limiting membrane; **FA** = fluorescein angiography; **GBM** = gradient boost machine; **GCIPL** = ganglion cell-inner plexiform layer; **HR** = hazard ratio; **INL** = inner nuclear layer; **IOP** = intraocular pressure; **RNFL** = retinal nerve fiber layer; **TABS** = Topcon Advanced Boundary Segmentation.

Keywords:
Retinal biomarker, Glaucoma, Prediction, Risk stratification.

Correspondence:
Danli Shi, MD, PhD, School of Optometry, The Hong Kong Polytechnic University, Kowloon, Hong Kong 999077. E-mail: danli.shi@polyu.edu.hk; and Mingguang He, MD, PhD, School of Optometry, The Hong Kong Polytechnic University, Kowloon, Hong Kong 999077. E-mail: mingguang.he@polyu.edu.hk.

References

1. Jonas JB, Aung T, Bourne RR, et al. Glaucoma. *Lancet*. 2017;390:2183−2193.
2. Bou Ghanem GO, Wareham LK, Calkins DJ. Addressing neurodegeneration in glaucoma: mechanisms, challenges, and treatments. *Prog Retin Eye Res*. 2024;100:101261.
3. King AJ, Hudson J, Azuara-Blanco A, et al. Evaluating primary treatment for people with advanced glaucoma: five-year results of the treatment of advanced glaucoma study. *Ophthalmology*. 2024;131:759−770.
4. Wang W, Wang H. Understanding the complex genetics and molecular mechanisms underlying glaucoma. *Mol Aspects Med*. 2023;94:101220.
5. Shi D, Lin Z, Wang W, et al. A deep learning system for fully automated retinal vessel measurement in high throughput image analysis. *Front Cardiovasc Med*. 2022;9:823436.
6. Ko F, Foster PJ, Strouthidis NG, et al. Associations with retinal pigment epithelium thickness measures in a large cohort: results from the UK biobank. *Ophthalmology*. 2017;124:105−117.
7. Chan KKW, Tang F, Tham CCY, et al. Retinal vasculature in glaucoma: a review. *BMJ Open Ophthalmol*. 2017;1:e000032.
8. Rudnicka AR, Owen CG, Welikala RA, et al. Retinal vasculometry associations with glaucoma: findings from the European prospective investigation of Cancer-Norfolk Eye Study. *Am J Ophthalmol*. 2020;220:140−151.
9. Lin TPH, Hui HYH, Ling A, et al. Risk of normal tension glaucoma progression from automated baseline retinal-vessel caliber analysis: a prospective cohort study. *Am J Ophthalmol*. 2023;247:111−120.
10. Andrade JCF, Kanadani FN, Furlanetto RL, et al. Elucidation of the role of the lamina cribrosa in glaucoma using optical coherence tomography. *Surv Ophthalmol*. 2022;67:197−216.
11. Shin JW, Sung KR, Park SW. Patterns of progressive ganglion cell-inner plexiform layer thinning in glaucoma detected by OCT. *Ophthalmology*. 2018;125:1515−1525.
12. Swaminathan SS, Jammal AA, Berchuck SI, Medeiros FA. Rapid initial OCT RNFL thinning is predictive of faster visual field loss during extended follow-up in glaucoma. *Am J Ophthalmol*. 2021;229:100−107.
13. Yusufu M, Weinreb RN, Kang M, et al. Structural and causal links between retinal vascular geometry and neural layer thickness. *Microvasc Res*. 2025;161:104834.
14. Ha A, Park KH. Optical coherence tomography for the diagnosis and monitoring of glaucoma. *Asia Pac J Ophthalmol (Phila)*. 2019;8:135−145.
15. Alarcon-Martinez L, Shiga Y, Villafranca-Baughman D, et al. Neurovascular dysfunction in glaucoma. *Prog Retin Eye Res*. 2023;97:101217.
16. Kancheva K, Radeva M, Resnick IB, Zlatarova Z. Evaluation of OCT angiography parameters as biomarkers for glaucoma progression. *Diagnostics (Basel)*. 2025;16:35.
17. Hsia Y, Chang H-L, Wang T-H, et al. The artifacts in macular and peripapillary OCT angiography in patients with different severities of glaucoma. *Ophthalmol Sci*. 2026;6:100964.
18. Lai C, Chuang LH, Lai CC, et al. Longitudinal changes in optical coherence tomography angiography characteristics in normal-tension glaucoma with or without high myopia. *Acta Ophthalmol*. 2024;102:e762−e773.
19. Yusufu M, Burton MJ, Jin S, et al. Retinomics: a window to multidisease prediction using retinal biomarkers from routine eye imaging. *BMC Med*. 2025;23:662.
20. Sudlow C, Gallacher J, Allen N, et al. UK biobank: an open access resource for identifying the causes of a wide range of complex diseases of middle and old age. *PLoS Med*. 2015;12:e1001779.
21. Chua SYL, Thomas D, Allen N, et al. Cohort profile: design and methods in the eye and vision consortium of UK Biobank. *BMJ Open*. 2019;9:e025077.
22. Ribeiro Reis AP, Ioannidou E, Wagner SK, et al. Retinal morphology across the menstrual cycle: insights from the UK Biobank. *NPJ Womens Health*. 2024;2:38.
23. von Elm E, Altman DG, Egger M, et al. The strengthening the reporting of observational studies in epidemiology (STROBE) statement: guidelines for reporting observational studies. *J Clin Epidemiol*. 2008;61:344−349.

24. Shi D, Zhou Y, He S, et al. Cross-modality labeling enables noninvasive capillary quantification as a sensitive biomarker for assessing cardiovascular risk. *Ophthalmol Sci*. 2024;4:100441.
25. Patel PJ, Foster PJ, Grossi CM, et al. Spectral-domain optical coherence tomography imaging in 67 321 adults: associations with macular thickness in the UK biobank study. *Ophthalmology*. 2016;123:829−840.
26. Wagner SK, Bountziouka V, Hysi P, Rahi JS. Associations between unilateral amblyopia in childhood and cardiometabolic disorders in adult life: a cross-sectional and longitudinal analysis of the UK Biobank. *EClinicalMedicine*. 2024;70:102493.
27. Yang Q, Reisman CA, Wang Z, et al. Automated layer segmentation of macular OCT images using dual-scale gradient information. *Opt Express*. 2010;18:21293−21307.
28. Yusufu M, Vingrys AJ, Shang X, et al. Population-based normative reference for retinal microvascular Atlas. *Ophthalmol Sci*. 2025;5:100723.
29. Zekavat SM, Raghu VK, Trinder M, et al. Deep learning of the retina enables Phenome- and genome-wide analyses of the microvasculature. *Circulation*. 2022;145:134−150.
30. Wu R, Cheung CY, Saw SM, et al. Retinal vascular geometry and glaucoma: the Singapore Malay Eye Study. *Ophthalmology*. 2013;120:77−83.
31. Miao S, Chen Q, Jiang Y, et al. Associations of retinal microvascular density and fractal dimension with glaucoma: a prospective study from UK Biobank. *Ophthalmol Sci*. 2024;5:100661.
32. Richter GM, Sylvester B, Chu Z, et al. Peripapillary microvasculature in the retinal nerve fiber layer in glaucoma by optical coherence tomography angiography: focal structural and functional correlations and diagnostic performance. *Clin Ophthalmol*. 2018;12:2285−2296.
33. Yarmohammadi A, Zangwill LM, Diniz-Filho A, et al. Relationship between optical coherence tomography angiography vessel density and severity of visual field loss in glaucoma. *Ophthalmology*. 2016;123:2498−2508.
34. Wu JH, Moghimi S, Nishida T, et al. Detection and agreement of event-based OCT and OCTA analysis for glaucoma progression. *Eye (Lond)*. 2024;38:973−979.
35. Canchi S, Guo X, Phillips M, et al. Role of Re-entry tears on the dynamics of type B dissection flap. *Ann Biomed Eng*. 2018;46:186−196.
36. Burns SA, Elsner AE, Gast TJ. Imaging the retinal vasculature. *Annu Rev Vis Sci*. 2021;7:129−153.
37. Chen DF, Wang C, Si Y, et al. Natural history and risk factors for glaucoma progression in Chinese patients with normal-tension glaucoma. *Invest Ophthalmol Vis Sci*. 2024;65:28.
38. Park SE, Lee JS, Kim M, et al. What are the factors associated with the structural damage differences in open-angle glaucoma? RNFL- and GCIPL-dominant progression. *J Clin Med*. 2022;11(22).
39. Wu K, Lin C, Lam AK, et al. Wide-field trend-based progression analysis of combined retinal nerve fiber layer and ganglion cell inner plexiform layer thickness: a new paradigm to improve glaucoma progression detection. *Ophthalmology*. 2020;127:1322−1330.
40. Vianna JR, Butty Z, Torres LA, et al. Outer retinal layer thickness in patients with glaucoma with horizontal hemifield visual field defects. *Br J Ophthalmol*. 2019;103:1217−1222.
41. Kim EK, Park HL, Park CK. Relationship between retinal inner nuclear layer thickness and severity of visual field loss in glaucoma. *Sci Rep*. 2017;7:5543.
42. Jung KI, Ryu HK, Oh SE, et al. Thicker inner nuclear layer as a predictor of glaucoma progression and the impact of intraocular pressure fluctuation. *J Clin Med*. 2024;13:2312.
43. Fan N, Huang N, Lam DS, Leung CK. Measurement of photoreceptor layer in glaucoma: a spectral-domain optical coherence tomography study. *J Ophthalmol*. 2011;2011:264803.
44. Hasegawa T, Akagi T, Yoshikawa M, et al. Microcystic inner nuclear layer changes and retinal nerve fiber layer defects in eyes with glaucoma. *PLoS One*. 2015;10:e0130175.
45. El Maftouhi A, Quaranta-El Maftouhi M, Baudouin C, Denoyer A. Cystic maculopathy of the inner nuclear layer in glaucoma patients. *J Fr Ophtalmol*. 2021;44:786−791.
46. Gordon MO, Torri V, Miglior S, et al. Validated prediction model for the development of primary open-angle glaucoma in individuals with ocular hypertension. *Ophthalmology*. 2007;114:10−19.
47. Mohammadzadeh V, Moghimi S, Nishida T, et al. Association of rates of ganglion cell and inner plexiform thinning with development of glaucoma in eyes with suspected glaucoma. *JAMA Ophthalmol*. 2023;141:349−356.
48. Shin JW, Sung KR, Song MK. Ganglion cell-inner plexiform layer and retinal nerve fiber layer changes in glaucoma suspects enable prediction of glaucoma development. *Am J Ophthalmol*. 2020;210:26−34.